than $M(II)XS_5^+$. That is to say because $ZnXS_5^+$ is a weaker hard acid than ZnS^{62+}, a decrease in K_2 from Cl to I (Figure 2) is smaller than that in K_1. On the other hand, because $CdXS_5^+$ is a stronger soft acid than CdS_6^{2+}, an increase in K_2 from Cl to I is larger than that in K_1. Thus, we conclude that the K_2/K_1 ratio increases in going from Cl to I.

Thiocyanate Complex. We have the following knowledge on the structure of cadmium thiocyanate complexes (cf. Introduction). The cadmium thiocyanate complexes seem not to change their structure, keeping a six-coordinated octahedral configuration, contrary to the zinc thiocyanate complexes. According to the previous discussion,[1] the zinc thiocyanate complexes have a four-coordinated tetrahedral structure; that is, the structural change from an octahedral to a tetrahedral configuration occurs at the formation of a monothiocyanate complex. Cd(II) may be partly coordinated through a sulfur atom (S-coordination) in methanol as in water, though Zn(II) is coordinated through a nitrogen atom of NCS^- (N-coordination).

As for the N- or S-coordination, it was reported that the change from M-NCS to M-SCN bonding coincides approximately in the periodic table with the change in relative binding of halide ions from $F^- > Cl^- > Br^- > I^-$ to $I^- > Br^- > Cl^- > F^-$.[23,24] Hence, it is probable that the existence of S-coordinated species in the cadmium thiocyanate complexes in methanol is supported by our results of halide complexes. If so, *S*-coordination may appear easily in complexes containing many NCS^- ions such as $Cd(CNS)_3S_3^-$ or $Cd(CNS)_4S_2^{2-}$ because the coordination of NCS^- probably increases the softness of Cd(II). According to a Raman study in water,[14] in $Cd(CNS)_4^{2-}$ (even in the complexes containing less NCS^-) some of the NCS^- is bound to Cd(II) through the N and some through the S.

In comparison with those of the iodide complexes, the stabilities of the thiocyanate complexes in methanol indicate some tendency similar to that in water: in water, at 25 °C and I = 0 M, log K_1(Zn-I) = -1.5 (I = 3.0 M), log K_1(Zn-NCS) = 1.33, log K_2(Zn-NCS) = 0.58, log K_1(Cd-I) = 2.28, log K_2(Cd-I) = 1.64, log K_1(Cd-NCS) = 1.89, log K_2(Cd-NCS) = 0.89[25] (cf. log K_1(Zn-I) = -2.93 and log K_2(Zn-I) = 1.17 at I = 4.5[26]). Why K_1(Zn-NCS) is large was previously explained by the structural change of zinc monothiocyanate. The results of K_1(Cd-I) > K_1(Cd-NCS) and K_2(Cd-I) > K_2(Cd-NCS) seem to be normal because Hg(II) of S-coordination also gives the same results in water: log K_1(Hg-I) = 12.87 (I = 0.5), log K_2(Hg-I) = 10.95 (I = 0.5), log K_1(Hg-NCS) = 9.08 (I = 1), log K_2(Hg-NCS) = 7.78 (I = 1).[25] However, considering K_1(Hg-NCS) > K_1(Hg-Cl) in water (log K_1(Hg-Cl) = 6.74 at I = 0.5), K_1(Cd-NCS) appears to be too small in methanol. This may support a prediction that the N-coordination dominantly exists in the cadmium monothiocyanate complex. As K_2(Zn-NCS) < K_2(Zn-I), we think that K_2(Zn-I) is too large if it is considered that the Zn-N bond is just slightly covalent (less than that in Zn-Br).[14] For this reason, it is thought that the zinc dihalide complex is stabilized significantly by the structural change.

The K_2/K_1 ratio of cadmium thiocyanate is considerably small, like those of its halides, 2.4×10^{-3}. Thus, if the cadmium thiocyanate complex changes its structure, the structural change in the tri- or tetrathiocyanate complex might be predicted. However, if there is no probability of structural change in the cadmium thiocyanate complex contrary to the zinc thiocyanate complex, we will expect that this structural property of cadmium thiocyanate is related to ambidentate binding of NCS^- to Cd(II).

Acknowledgment. C.Y. and H.O. thank Associate Professor Shigeo Sawada of Kinki University for his kind direction. K.N.S. thanks Professor Dr. Ko Ko Gyi of Rangoon University, Rangoon, Burma, for his kind permission to do research work in Japan.

(23) Lindquist, I.; Standberg, B. *Acta Crystallogr.* **1957**, *10*, 173.
(24) Mitchell, P. C. H.; Williams, R. J. P. *J. Chem. Soc.* **1960**, 1912.
(25) Smith, R. M.; Martell, A. E. *Critical Stability Constants*; Plenum: New York, 1976; Vol. 4.
(26) Shchukarev, S. A.; Lilich, L. S.; Latysheva, V. A. *Russ. J. Inorg. Chem.* (*Engl. Transl.*) **1956**, *1*(2), 36.

Contribution from the Research School of Chemistry, Australian National University, Canberra, ACT 2601, Australia, and Chemistry Department, University of Tasmania, Hobart, Tasmania 7001, Australia

Electronic Spectrum of $Cs_3Mo_2Cl_9$

Lucjan Dubicki,*† Elmars Krausz,‡ Robert Stranger,§ Peter W. Smith,§ and Yukito Tanabe∥

Received December 10, 1986

The single-crystal absorption, MCD, and Zeeman spectra are reported for $Cs_3Mo_2Cl_9$. The highly structured absorption at ~13 000 cm^{-1} has no MCD and consists of spin-singlet and orbitally nondegenerate states. New absorption lines are observed near 11 600 and 7800 cm^{-1}. The main spectroscopic features can be qualitatively explained on the basis of an exchange-coupled-pair model with strong σ Mo-Mo bonding. The σ bonding preferentially stabilizes the pair states derived from the $t_{2e}^2t_{2e}^2$ configuration. However, the t_{2z} electrons are not fully paired and the ground singlet-triplet separation is dominated by t_{2z}-t_{2z} kinetic exchange. The bonding in $Mo_2Cl_9^{3-}$ and $W_2Cl_9^{3-}$ is considered to be qualitatively the same, with one strong σ bond and two weak π interactions.

Introduction

The anion of the title compound is a member of the classic series $M_2X_9^{3-}$ (M(III) = Cr, Mo, W; X = Cl, Br) in which the strength of the M-M bonding is reflected in the structural distortions of the bridging group and a progressive reduction in M-M separations.[1-4] Direct Cr-Cr bonding is very weak and the ground singlet-triplet separation[5] is very small, $E_{10} \sim 13$ cm^{-1}. $Cs_3Mo_2Cl_9$ is weakly paramagnetic. The magnetic susceptibility[5] can be fitted to either a d^3d^3, d^2d^2, or d^1d^1 model and gives $E_{10} \sim 840$ cm^{-1}. The $W_2Cl_9^{3-}$ anion is diamagnetic[6] at 298 K. The changes in the structural and magnetic properties have been interpreted[7] by assigning no M-M bonds in $Cr_2Cl_9^{3-}$, one bond in $Mo_2Cl_9^{3-}$, and three bonds in $W_2Cl_9^{3-}$.

The electronic spectra of $Cr_2X_9^{3-}$ have been studied by many workers.[8-10] The exchange interactions are small and together

† Visiting Fellow, Research School of Chemistry, Australian National University.
‡ Australian National University.
§ University of Tasmania.
∥ Present address: Department of Applied Physics, University of Tokyo, Tokyo, Japan

(1) Wessel, G. J.; Ijdo, D. J. W. *Acta Crystallogr.* **1957**, *10*, 466.
(2) Watson, W. H., Jr.; Waser, J. A. *Acta Crystallogr.* **1958**, *11*, 689.
(3) Saillant, R.; Jackson, R. B.; Streib, W. E.; Folting, K.; Wentworth, R. A. D. *Inorg. Chem.* **1971**, *10*, 1453.
(4) Cotton, F. A.; Ucko, D. A. *Inorg. Chim. Acta* **1972**, *6*, 161.
(5) Grey, I. E.; Smith, P. W. *Aust. J. Chem.* **1971**, *24*, 73.
(6) Saillant, R.; Wentworth, R. A. D. *Inorg. Chem.* **1968**, *7*, 1606.
(7) Summerville, R. H.; Hoffmann, R. *J. Am. Chem. Soc.* **1979**, *101*, 3821.

0020-1669/87/1326-2247$01.50/0

Table I. Skeletal Vibrations in $Cs_3M_2Cl_9$ Complexes[a]

		$Cs_3Cr_2Cl_9$[b]	$Cs_3Mo_2Cl_9$[c]
terminal str	ν_1 A_1'	378	350
	ν_8 E'	346	333
	ν_{13} E''	337	298
	ν_5 A_2''	340	320
bridging str	ν_2 A_1'	283	
	ν_6 A_2''	256	240
	ν_9 E'	234	273
	ν_{14} E''	199	239
terminal bend	ν_3 A_1'	200	217
	ν_{10} E'	193	180
	ν_7 A_2''	184	152
	ν_{15} E''	172	
	ν_{11} E'	161	165
bridging bend	ν_{16} E''	145	138[d]
	ν_4 A_1'	138	143[d]
	ν_{12} E'	75	92

[a] The assignments and notation are those of Black et al.[16] [b] Single-crystal data.[16] [c] Microcrystalline data.[17] [d] The E'' and A_1' assignments are uncertain and may be interchanged.

with spin–orbit coupling and a trigonal field produce a rich multiplet fine structure. However the multiplet energies are mainly determined by the cubic field and the electron repulsion energies, and consequently $Cr_2X_9^{3-}$ is an excellent example of a weakly coupled pair.

In $Mo_2Cl_9^{3-}$ there is at least one strong interaction between the t_{2z} orbitals, which are optimized for σ Mo–Mo bonding. The electronic spectrum of $Mo_2Cl_9^{3-}$ has not been analyzed, and the consequences of a strong σ bond have not been properly explored.[11,12] We have examined the electronic spectrum of $Cs_3Mo_2Cl_9$ with Zeeman and MCD experiments and have used the exchange-coupled-pair model to assign the energy levels.

Experimental Section

Preparation of Crystals. Stoichiometric quantities of CsCl and $MoCl_3$ were dried under vacuum in a silica tube heated at 140 °C for 24 h. The tube was sealed and held in a furnace at 950 °C for 4–6 days. The tube was slowly cooled, yielding red brown hexagonal plates and prisms. The plates contained the well-developed (001) face with a surface area of 1–2 mm^2 and were used for axial and MCD spectra. The hexagonal rods had a smaller surface area and were used for orthoaxial spectra.

Crystals of $Cs_3Mo_2Cl_9$ have the space group D_{6h}^4–$P6_3/mmc$ and Z = 2. The crystal structure[3] consists of discrete confacial bioctahedra ($Mo_2Cl_9^{3-}$). The close packing of the ions and the influence of the cation size on the geometry of the anion are discussed in a recent publication.[31]

Spectroscopic Measurements. The equipment used for absorption, MCD, and Zeeman experiments was the same as described elsewhere[13] except the BOC cryostat was replaced by an Oxford Instruments SM4 superconducting solenoid cryostat.

Vibrational Spectra. The vibrational spectra of $A_3M_2X_9$ compounds have been examined by many authors.[14-16] Recent work[17] has compared the powder spectra of a series of alkali-metal, ammonium, and alkylammonium salts of $Mo_2X_9^{3-}$ (X = Cl, Br, I). Table I compares the vibrational frequencies of $Cs_3Mo_2Cl_9$ with those of $Cs_3Cr_2Cl_9$. For simplicity, the factor group splittings (~4 cm^{-1} in $Cs_3Cr_2Cl_9$) of the E' vibrations are neglected. The internal vibrations can be approximately classified into four groups, terminal stretches, bridging stretches, terminal bending, and bridging bending. Of particular interest are the A_1' vibrations, three of which exhibit exchange striction in $Cs_3Cr_2Cl_9$.[18] The exception is the bridging stretching mode at 285 cm^{-1}, which apparently does not involve a large Cr–Cr displacement. Note that three of the groups have E', E'', and A_2'' members, so that the σ and π false origins in the electronic spectrum may be closely spaced. In addition to the internal vibrations there are a large number of lattice vibrations,[16,17] some of which appear to be vibronically active in the electronic spectrum (vide infra).

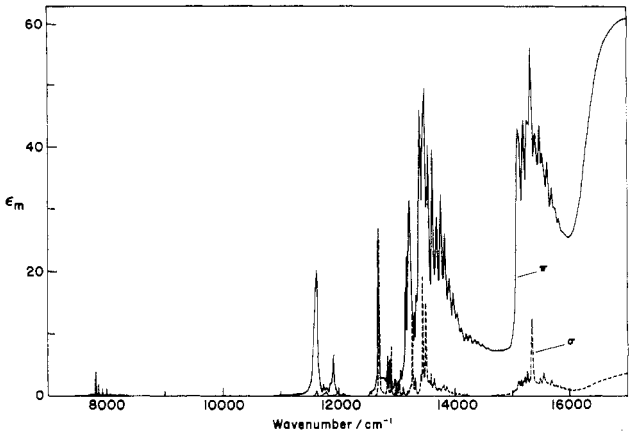

Figure 1. Single-crystal absorption spectra of $Cs_3Mo_2Cl_9$ at 15 K: solid line, π polarization; dashed line, σ polarization.

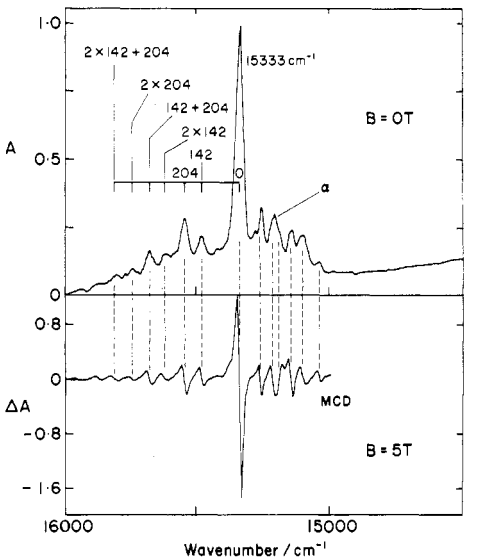

Figure 2. Axial absorption and MCD spectra of the 15 300-cm^{-1} band of $Cs_3Mo_2Cl_9$ at 6 K.

Electronic Absorption Spectrum. General Spectral Features. The low-resolution spectrum is given in Figure 1. The absorption beyond 17 000 cm^{-1} is very intense in z polarization. In addition to the known absorptions at 15 300 and 13 500 cm^{-1} we find new lines near 11 600 and 7800 cm^{-1}. The latter are mainly σ polarized. The absorption and MCD measurements were extended to 4000 cm^{-1}, and no other lines were detected. A number of spectroscopic measurements were limited by the lack of sufficiently thick crystals. In particular we were not able to measure accurate magnetic g factors for the very weak σ lines near 11 600 cm^{-1}. No emission was detected to 2.4 μm, with Ar^+ excitation, although the crystal used was quite small, thus limiting the sensitivity.

Absorption near 15 300 cm^{-1}. Figure 2 gives the MCD and axial absorption spectrum. No Zeeman splittings were resolved because of a large bandwidth, $\bar{\nu}_{1/2} \sim 25$ cm^{-1}. For the best resolved line at 15 333 cm^{-1} (σ) the g factor is estimated to be +0.6 to +1.0. This value is significantly lower than the spin-only value and suggests that the magnetic moment originates from orbital degeneracy, i.e. $^1E' \leftarrow {}^1A_1'$.

The fine structure above 15 333 cm^{-1} consists of progressions in 204- and 142-cm^{-1} vibrations, which may be assigned to $\nu_3(A_1')$ and $\nu_4(A_1')$ (Table I). The lower energy fine structure is based on a weak origin at

(8) Dubicki, L.; Ferguson, J.; Harrowfield, B. V. *Mol. Phys.* **1977**, *34*, 1545.
(9) Briat, B.; Russel, M. F.; Rivoal, J. C.; Chapelle, J. P.; Kahn, O. *Mol. Phys.* **1977**, *34*, 1357.
(10) Dean, N. J.; Maxwell, K. J.; Stevens, K. W. H.; Turner, R. J. *J. Phys. C* **1985**, *18*, 4505.
(11) Saillant, R.; Wentworth, R. A. D. *Inorg. Chem.* **1969**, *8*, 1226.
(12) Trogler, W. C. *Inorg. Chem.* **1980**, *19*, 697.
(13) Krausz, E.; Ludi, A. *Inorg. Chem.* **1985**, *24*, 939.
(14) Ziegler, R. J.; Risen, W. M., Jr. *Inorg. Chem.* **1972**, *11*, 2796.
(15) Beattie, I. R.; Gilson, T. R.; Ozin, F. A. *J. Chem. Soc. A* **1968**, 2765.
(16) Black, J. D.; Dunsmuir, J. T. R.; Forrest, I. W.; Lane, A. P. *Inorg. Chem.* **1975**, *14*, 1257.
(17) Smith, P. W.; Stranger, R. *Aust. J. Chem.* **1986**, *39*, 1269.
(18) Johnstone, I. W.; Briat, B.; Lockwood, D. J. *Solid State Commun.* **1980**, *35*, 689.

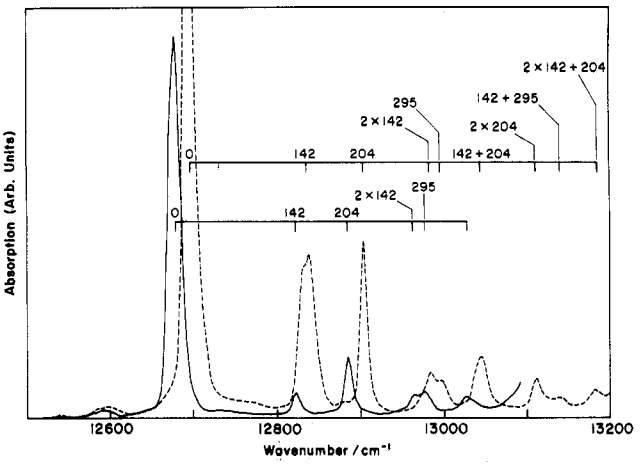

Figure 3. Orthoaxial absorption spectra in the 12 600–13 100-cm^{-1} region of $Cs_3Mo_2Cl_9$ at 6 K: solid line, π polarization; dashed line, σ polarization.

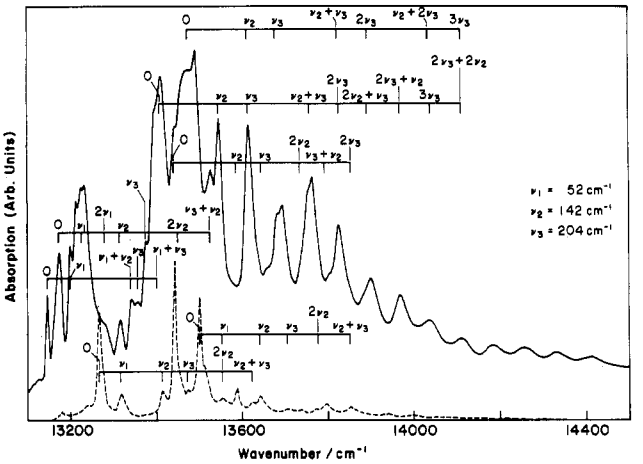

Figure 4. Orthoaxial absorption spectra in the 13 100–14 400-cm^{-1} region of $Cs_3Mo_2Cl_9$ at 6 K: solid line, π polarization; dashed line, σ polarization.

15 032 cm^{-1}. A detailed analysis is complicated by the possible factor group splittings of both the electronic and vibrational levels. For example, an E′ electronic level gives E_{2g} and E_{1u} factor group components, both of which may be allowed through a vibronic mechanism.

Absorption near 13 300 cm^{-1}. The spectrum in the region 12 500–14 500 cm^{-1} shows no Zeeman splittings even for the sharp lines ($\bar{\nu}_{1/2}$ < 5 cm^{-1}), which occur at 13 148 and 13 341 cm^{-1} in π polarization. Furthermore, the axial spectrum has no MCD. We estimate $\Delta A/A$ < 0.003 and hence g < 0.01. The electronic states cannot have any spin or orbital magnetic moments, and the entire σ absorption must be vibronically induced through an E vibration.

The fine structure in the 12 600–13 100-cm^{-1} region (Figure 3) consists of progressions in 142-, 204-, and possibly 295-cm^{-1} modes, on the basis of two origins at 12 695 (σ) and 12 679 cm^{-1}(π). Since the σ line must be a false origin with one quantum of an E vibration, the neighboring π line is probably a false origin as well.

Most of the structure at higher energy (Figure 4) is also due to progressions in 142- and 204-cm^{-1} modes. The σ spectrum has three prominent (false) origins at 13 494, 13 439, and 13 265 cm^{-1}, which may involve one quantum of ν_8, ν_9, and ν_{12} E′ vibrations, respectively (Table I).

The π spectrum has similar origins at 13 474 and 13 397 cm^{-1}, and it is tempting to assign them as false origins involving one quantum of ν_5 and ν_6 A_2'' modes. From Table I we expect to see no π analogue of the third σ origin. Indeed the π spectrum contains a series of closely spaced lines in the range 13 148–13 233 cm^{-1} and suggests strong vibronic activity by lattice modes. We have not been able to locate the true origins, and at present, a consistent interpretation of the σ and π fine structure has not been achieved.

Absorption near 11 600 cm^{-1}. The absorption bands are broad, and no Zeeman splitting is resolved either in π or σ polarization (Figure 5). The π origin at 11 616 cm^{-1} has $\bar{\nu}_{1/2} \sim 50$ cm^{-1} and is associated with satellites at 143, 204, 266(sh), 309 and 345 (sh) cm^{-1}. Most of the satellites are probably vibronics, involving A_1' vibrations (Table I).

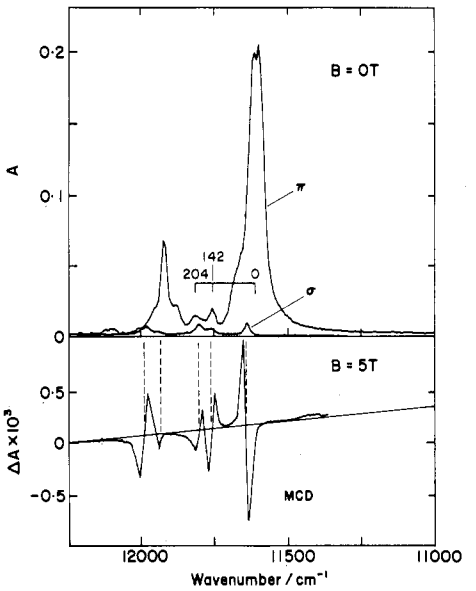

Figure 5. Orthoaxial absorption and MCD spectra of $Cs_3Mo_2Cl_9$ near 11 600 cm^{-1} at 6 K.

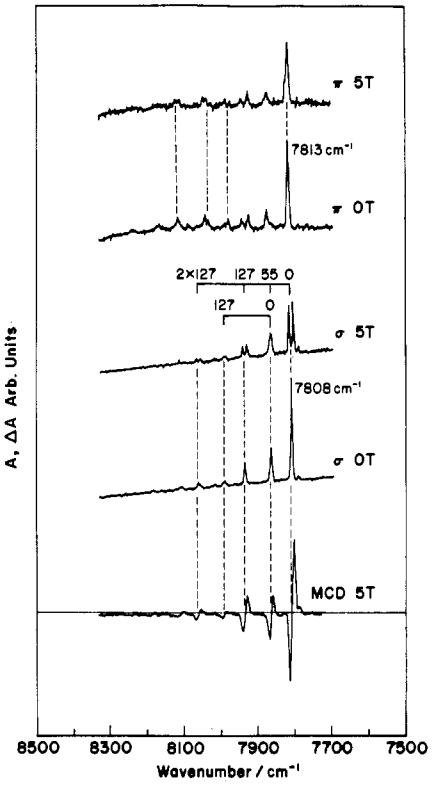

Figure 6. Transverse Zeeman and MCD spectra of $Cs_3Mo_2Cl_9$ near 7800 cm^{-1} at 6 K. The applied magnetic field was $B||Z$, in all cases. The dashed lines in the π spectra label lines with large Zeeman splitting, $|g| \simeq 2.5$ (see text).

The σ spectrum is very weak. The σ origin at 11 639 cm^{-1} has a positive g value. Assuming a gaussian line shape, the observed parameters $\Delta A/A \sim 0.6$ and $\bar{\nu}_{1/2} \sim 19$ cm^{-1} give $g_z \sim +2$. However it is difficult to measure A and $\bar{\nu}_{1/2}$ with any precision, and the error in g may be large. Most of the higher energy σ lines have negative g values, and if they are vibronics based on the σ origin, then they must involve E vibrations. In the absence of accurate g values we cannot ignore the possibility of other electronic states lying near ~11 925 cm^{-1}.

Absorption near 7800 cm^{-1}. The σ spectrum has a sharp origin at 7808 cm^{-1} with $g_z = -2.5$ (Figure 6). A second origin occurs at 7863 cm^{-1} with $g_z = -0.8$. The remaining fine structure involves progressions in a 127-cm^{-1} vibration. The latter does not change the sign or the magnitude of the g values and behaves as a totally symmetric vibration. The obvious assignment is $\nu_4(A_1')$, although the frequency is significantly different from the value of 142 cm^{-1} observed for the higher energy states.

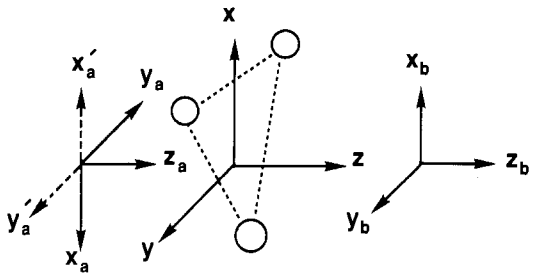

Figure 7. Coordinate axes for $Cs_3Mo_2Cl_9$ (see text).

The π origin occurs at 7813 cm^{-1}. The transverse Zeeman spectrum (field along z axis) can be simply explained on the basis of a pair of A_1'' and A_2'' levels with a zero-field splitting of ~ 5 cm^{-1} ($E(A_1'') > E(A_2'')$) and $|g_z| = 1.35$. The π fine structure is very weak. Three lines have large splittings with $|g_z| = 2.5$ and are indicated by dotted lines in Figure 6. They are assigned as vibronics of the first σ origin, $E' \times Q(E'')$. The energy separations then give 308, 223, and 169 cm^{-1} for the frequencies of the E'' vibrations. The remaining lines have smaller Zeeman splittings and we are unable to distinguish between vibronics of the type $(A_1'' + A_2'') \times Q(A_1')$ and $E'(g_z = -0.8) \times Q(E'')$. The theoretical implications of these Zeeman spectra are examined in the Discussion.

Theory

Exchange Hamiltonian. The optical spectrum of $Cs_3Mo_2Cl_9$ exhibits a series of distinct low-energy multiplets. The molecular orbital model is of limited use in this case since configuration interaction is expected to be very extensive. We adopt the exchange-coupled-pair model and use the formalism and notation of Tanabe and Fuchikami.[19-21]

The effective exchange Hamiltonian[20,21] to the second order in perturbation energy is

$$\mathbf{H}_{ex} = \sum_{a(\alpha\alpha')b(\beta\beta')} \sum \{[K(\alpha\alpha',\beta\beta') - J(\alpha\alpha',\beta\beta')/2] \times n_a(\alpha\alpha')\, n_b(\beta\beta') - 2J(\alpha\alpha',\beta\beta')\, S_a(\alpha\alpha')\cdot S_b(\beta\beta') + n_a(\alpha\alpha')\, \delta(\beta\beta') J(b\leftarrow a) + n_b(\beta\beta')\, \delta(\alpha\alpha') J(a\leftarrow b)\} \quad (1)$$

where the localized orbitals α and β belong to metal ions a and b, respectively. The generalized occupation number and spin operator are defined as

$$n(\alpha\alpha') = \sum_{\sigma} a^{+}_{\alpha\sigma} a_{\alpha'\sigma} \qquad \mathbf{S}(\alpha\alpha') = \sum_{\sigma,\sigma'} \langle\sigma|\mathbf{s}|\sigma'\rangle a^{+}_{\alpha\sigma} a_{\alpha'\sigma'} \quad (2)$$

The leading terms in the expressions for the effective parameters are

$$K(\alpha\alpha',\beta\beta') = \langle\alpha(1)\ \beta(2)|g|\alpha'(1)\ \beta'(2)\rangle \quad (3)$$

$$-2J(\alpha\alpha',\beta\beta') = -2\langle\alpha\beta|g|\beta'\alpha'\rangle + 4h(\alpha\leftarrow\beta')h(\beta\leftarrow\alpha')/U \quad (4)$$

$$J(b\leftarrow a) = -h(\alpha\leftarrow\beta')h(\beta\leftarrow\alpha')/U \quad (5)$$

where g is the Coulomb energy operator and $h(\alpha,\beta)$ is the transfer or hopping integral. Equation 4 gives the familiar spin-dependent exchange parameter, consisting of potential and kinetic exchange terms. For orbitals that are not singly occupied it is necessary to include the spin-independent terms, which include the Coulomb integrals (eq 3) and kinetic exchange (eq 5). In our calculations that employed the "kinetic exchange approximation" (vide infra) the spin-independent terms had only a minor effect on the energies of the lower lying pair states.

Trigonal Basis. The coordinate axes for the $M_2X_9^{3-}$ pair are shown in Figure 7. The orbital functions are defined with respect to (X_a, Y_a, Z_a) and (X_b, Y_b, Z_b) axes, so that the same transformation connects the cubic and trigonal basis at each center. The spin functions and all operators are defined with respect to the matched set of axes. This interpretation[22] is equivalent to that of earlier work.[23]

If ξ', η', ζ', u', and v' are real d orbitals defined with respect to trigonal axes, (X_a, Y_a, Z_a) or (X_b, Y_b, Z_b), then in the limit of local O_h symmetry the t_{2g} and e_g orbitals that diagonalize the cubic field are

$$t_{2x} = (2^{1/2}v' - \eta')/3^{1/2}$$

$$t_{2y} = -(2^{1/2}\zeta' + \xi')/3^{1/2}$$

$$t_{2z} = u'$$

$$e_x = (2^{1/2}\eta' + v')/3^{1/2}$$

$$e_y = (2^{1/2}\xi' - \zeta')/3^{1/2} \quad (6)$$

The corresponding M–M overlaps are

$$\langle t_{2x}|t_{2x}\rangle = \langle t_{2y}|t_{2y}\rangle = (S_\pi + 2S_\delta)/3$$

$$\langle t_{2z}|t_{2z}\rangle = S_\sigma$$

$$\langle e_x|e_x\rangle = \langle e_y|e_y\rangle = (2S_\pi + S_\delta)/3$$

$$\langle t_{2x}|e_x\rangle = \langle t_{2y}|e_y\rangle = -2^{1/2}(S_\pi - S_\delta)/3 \quad (7)$$

The local field of the terminal and bridging chloride ions is expected to generate a large cubic field. For example,[24] electronic spectra give $10Dq \sim 19000$ cm^{-1} for the monomeric species $MoCl_6^{3-}$. We therefore ignore e_g orbitals and choose an orthogonal set of t_2 orbitals, t_{2x}^0, t_{2y}^0, and t_{2z}^0 which resemble the orbitals in (6) but of course contain admixtures of ligand orbitals.[25,26]

$t_2^3t_2^3$ Multiplet. Within the exchange-coupled-pair model, strong bonding is represented by large transfer integrals and hence large kinetic exchange. We neglect all terms in (1) except those containing the transfer integrals $h(z,z)$ and $h(x,x) = h(y,y)$, where we have used the simplified notation t_{2x}^0, t_{2y}^0, $t_{2z}^0 = x, y, z$. We define

$$J_\sigma = 4h(z,z)^2/U$$

$$J_\pi = 36h(x,x)^2/U \quad (8)$$

where J_π corresponds, in local O_h symmetry, to bonding between orbitals fully optimized for π bonding, i.e. $J_\pi \sim 4h(\xi'_0,\xi'_0)^2/U$. The above "kinetic approximation" enables all the parameters in (4) and (5) to be expressed in terms of J_σ and J_π

$$-2J(z,z) \simeq J_\sigma$$

$$-2J(x,x) \simeq J_\pi/9$$

$$-2J(xz,zx) \simeq (J_\sigma J_\pi)^{1/2}/3$$

$$J(b\leftarrow a)_\sigma \simeq -J_\sigma/4$$

$$J(b\leftarrow a)_\pi \simeq -J_\pi/36 \quad (9)$$

The transfer integrals are related to molecular orbital energies.[27] Extended Huckel calculations[7] show that $h(z,z)$ is mainly determined by a σ Mo–Mo interaction. However both Mo–Cl and π Mo–Mo interactions contribute to $h(x,x)$, with opposite signs. In fact, Summerville and Hoffmann[7] argue that the positive contribution from Mo–Cl–Mo bonding cancels the direct interaction, giving no π bonds; i.e., J_π is very small.

We ignore spin–orbit coupling and single-ion trigonal fields as their contribution to multiplet energies is essentially quenched for large J_σ. However, it is necessary to include all the pair states

(19) Fuchikami, N.; Tanabe, Y. *J. Phys. Soc. Jpn.* **1979**, *47*, 505.
(20) Shigi, H.; Tanabe, Y. *J. Phys. Soc. Jpn.* **1982**, *51*, 1415.
(21) Fuchikami, N.; Block, R. *Physica B+C (Amsterdam)* **1983**, *119B+C*, 252.
(22) Leuenberger, B.; Güdel, H. U. *Mol. Phys.* **1984**, *51*, 1.
(23) Dubicki, L.; Tanabe, Y. *Mol. Phys.* **1977**, *34*, 1531.
(24) Smith, P. W.; Wedd, A. G. *J. Chem. Soc. A* **1970**, 2447.
(25) Gondaira, K.; Tanabe, Y. *J. Phys. Soc. Jpn.* **1966**, *21*, 1527.
(26) Barry, K. R.; Maxwell, K. J.; Siddiqui, K. A.; Stevens, K. W. H. *J. Phys. C.* **1981**, *14*, 1281.
(27) Hay, P. J.; Thibeault, J. C.; Hoffmann, R. *J. Am. Chem. Soc.* **1975**, *97*, 4884.

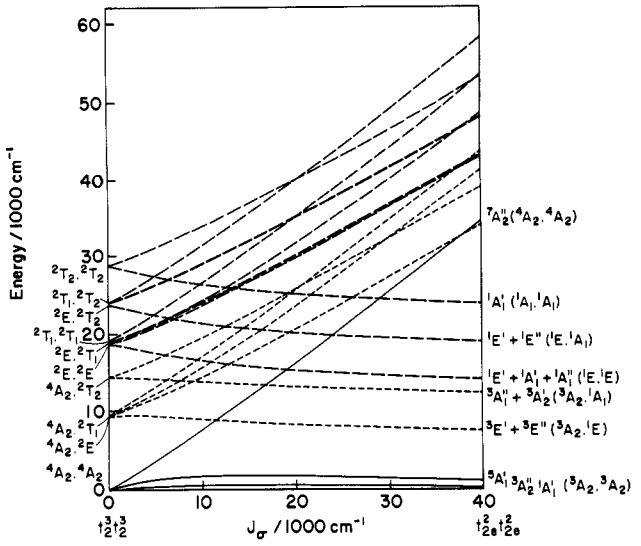

Figure 8. Calculated energy levels for the $t_2^3t_2^3$ configuration, with $J_\pi = 0$, $B = 410$, $C = 4B$, and $Dq = 1920$ cm^{-1}. The solid lines are ground-state pair states with $S = 1, 2, 3$, the close dashed lines are singly-excited states with $S = 1$ and the wide dashed lines are doubly excited pair states having $S = 0$ (see text for details). All singly excited $S = 2$ and doubly excited $S = 1$ levels move sharply to higher energy with increasing J_σ.

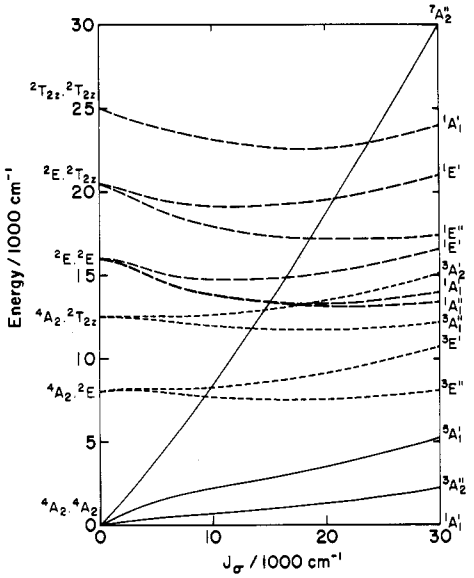

Figure 9. Calculated energy levels for the $t_2^3t_2^3$ configuration. The parameters are the same as in Figure 8 except $J_\pi = J_\sigma/4$.

derived from the $t_2^3t_2^3$ configuration. The Racah parameters are smaller for second-row metal ions, and the relatively low energies of doubly excited states are comparable to the matrix elements of (1) connecting the doubly excited level with the ground and singly excited levels. The appendixes give further details of the calculation. The variation of the energy levels with J_σ and J_π is displayed in Figures 8–10.

Magnetic *g* Factors. The matrix elements of angular momentum, L_z, were calculated by using standard methods.[28] For $J_\sigma > 5000$ cm^{-1}, the calculated orbital g_z factors for the lowest E states were, $g_0(^3E') = g_0(^3E'') = +2.0k$ and $g_0(^1E') = +4.0k$, where k is the orbital reduction parameter. In this regime the orbital g factors are independent of spin–orbit coupling, trigonal fields, and the Coulombic contribution to the splitting of the single-ion levels $t_2^3(^2E)$ and $t_2^3(^2T_1)$.

Even for $J_\sigma \simeq 1000$ cm^{-1}, there is a large orbital magnetic moment, and we obtain $g_0(^3E',^3E'') \simeq +1.8k$ and $g_0(^1E') \simeq +3.8k$.

(28) Griffith, J. S. *The Irreducible Tensor Method for Molecular Symmetry Groups*; Prentice Hall: Englewood Cliffs, NJ, 1962.

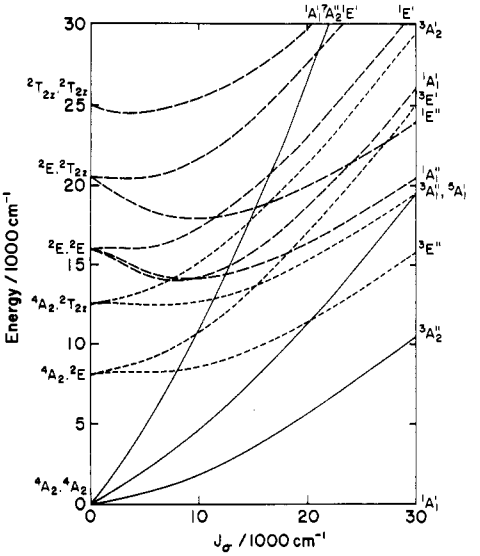

Figure 10. Calculated energy levels for the $t_2^3t_2^3$ configuration. The parameters are the same as in Figure 8 except $J_\pi = J_\sigma$.

Table II. Transition Electric Dipole for $^3E'$, $^3E'' \leftarrow {}^1A_1'$ Transitions[a]

	spinor $\|MM_s\rangle$[b]	
	$E''\ \|\pm1\,\pm1\rangle$	...
$^3E'$	$E'\ \|\pm1\ 0\rangle$	$R^{\pm}_{0\pm}/3^{1/2}$
	$A_1'' + A_2''\ \|\pm1\,\mp1\rangle$	$R^{z}_{\mp\pm}/3^{1/2}$
	$E'\ \|\pm1\,\pm1\rangle$	$R^{\mp}_{\pm\pm}/3^{1/2}$
$^3E''$	$E''\ \|\pm1\ 0\rangle$	...
	$A_1' + A_2''\ \|\pm1\ \mp\ 1\rangle$	...

[a] Taken from reference 23. The parameters $R_{\beta\gamma}{}^{\alpha}$ are defined in the text. [b] The orbital components M transform as $\mp(x \pm iy)/2^{1/2}$ for $^3E'$ and $\mp(L_x \pm iL_y)/2^{1/2}$ for $^3E''$, in the D_{3h} point group.

The extensive mixing of $|^4A_2{}^2T_1,{}^3E\rangle$ and $|^4A_2{}^2E,{}^3E\rangle$ states, caused by J_σ, is observed in a recent spectroscopic study of a tris(hydroxy)-bridged dimer of Cr(III),[34] where $J_\sigma \simeq 2000$ cm^{-1}.

Discussion

Single Excitations. Figure 8 indicates that the lines at 7800 cm^{-1} are due to $^3E \leftarrow {}^1A_1'$ transitions. The selection rules for a static electric dipole mechanism[23] are given in Table II. The transition dipole is $R_{\beta,\gamma}{}^{\alpha}$ where α is the polarization, β and γ are the changes in spin and orbital angular momenta, respectively, and $\alpha \equiv \beta + \gamma$, mod (3). For a vibronic mechanism we require $R_{\beta,\gamma,\delta}{}^{\alpha}$ where δ is the change in vibrational angular momentum and $\alpha \equiv \beta + \gamma + \delta$, mod (3). The σ line at 7808 cm^{-1} (Figure 6) can be assigned to the $^3E''(E') \leftarrow {}^1A_1'$ transition, so that $g_z = -2.5 = -(g_0 + g_s)$. Assuming $g_s \simeq 2$, we obtain $g_0 = +0.5$. Theoretically we expect $g_0 \simeq 2k$ so that $k \simeq 0.3$. The remaining spin–orbit components of $^3E''$ are statically forbidden.

The σ line at 7863 cm^{-1} has $g_z = -0.8$. This is not consistent with the positive g_0 predicted by theory. We have to assign this line as a vibronic involving one quantum of an E vibration. We cannot discriminate between the $E' \times Q(E')$ and $E'' \times Q(E'')$ assignments and therefore cannot establish whether the line is derived from $^3E''$ or $^3E'$ states.

The π line at 7813 cm^{-1} (Figure 6) behaves as a $A_2'' + A_1''$ spin–orbit "doublet" with a zero-field splitting of $\sim$5 cm^{-1} and $|g_z| = 1.35$. An obvious assignment (Table II) is the $^3E'(A_1'' + A_2'') \leftarrow {}^1A_1'$ transition, which has $|g_z| = |g_0 - g_s|$ so that $g_0 \simeq 2k \simeq 0.65$. However we cannot dismiss the possibility that the π line is a false origin, e.g. $(A_1' + A_2') \times Q(A_2'')$. An analysis of hot vibronic lines was not successful. Several features were observed at higher temperatures, but they were very weak and broad.

If the σ and π lines at 7808 and 7813 cm^{-1} are true origins then J_π is very small. If the π line is a false origin then the $^3E'$ levels should lie at higher energy (Figures 9 and 10), but we see no absorption up to 11 600 cm^{-1}.

Table III. Comparison between Observed and Calculated Energies

calcd energy,[a] cm^{-1}	species	origins,[b] cm^{-1}
0	$^1A_1'$	
527	$^3A_2''$	840[c]
1721	$^5A_1'$	
7409	$^3E''$	7808 (E')
7578	$^3E'$	7813 ($A_2'' + A_1'$)
11866	$^3A_1''$	11616 (A_2''), 11639 (E')
12064	$^3A_2'$	
12299	$^7A_2''$	
13697	$^1A_1'$	12679 (A_2''), 12695 (E') vibr
13698	$^1A_1''$	13265 (E') vibr
13945	$^1E'$	15032 (E')
		15333 (E') vibr

[a] Calculated energies for the lower lying states of the $t_2^3t_2^3$ configuration, with $J_\sigma = 15000$, $J_\pi = 600$, $B = 410$, $C = 4B$, and $D_q = 1920$ cm^{-1}. [b] The origins and some of the prominent vibronics are listed. The observed spin–orbit symmetry species are given in parentheses. [c] Obtained from magnetic susceptibility measurements.[5]

According to Figure 8 a large energy gap, ~4500 cm^{-1}, separates the first and second excited multiplets. The latter consists of $^3A_1''$ and $^3A_2'$ states, which are mainly derived from $^4A_2{}^2T_{2z}$ and $^2T_{1z}{}^2T_{2z}$ pair states. Two spin–orbit components are allowed by a static electric dipole mechanism[23], $^3A_1''(E')$ in σ with $g_z = 2$ and $^3A_1''(A_2'')$ in π polarization. The lines at ~11 600 cm^{-1} are assigned to $^3A_1''(A_2'',E') \leftarrow {}^1A_1'$ transitions.

Double Excitations. The next multiplet consists of $^1E'$, $^1A_1'$, and $^1A_1''$ states that are derived from the $^2E^2E$, $^2E^2T_1$, and $^2T_1{}^2T_1$ double excitations. They include spin and orbital singlets that have no MCD. We must assign the entire absorption in the 12 600–14 000-cm^{-1} region to $^1A_1', {}^1A_1'' \leftarrow {}^1A_1'$ transitions. Our tentative analysis of the spectrum (vide supra) suggests that the extensive fine structure is largely due to vibrational progressions based on several false origins, and the number of true origins may indeed be small.

The assignment of the moderately intense π lines to orbitally forbidden double excitations is not unprecedented. An excellent example of a vibronic exchange-induced electric dipole is observed[29] in the basic rhodo ion, $(NH_3)_5CrOCr(NH_3)_5^{4+}$. In this case double excitations gain intensity from an intense z-polarized transition lying only ~10 000 cm^{-1} to higher energy. This transition probably involves both Cr ↔ Cr and O → Cr electron transfers. Incidentally, the multiplet splittings in basic rhodo could not be quantitatively fitted with the spin-dependent forms of $\mathbf{H}_{ex}$. We now find that large spin independent terms, $n_a(\alpha\alpha)n_b(\beta\beta')$, connect the $^2E(A_1)^2E(A_1)$ and $^2T_1(A_2)^2T_1(A_2)$ pair states, and their inclusion improves the fit between theory and experiment.

The accidental degeneracy of the $^1E'$, $^1A_1'$, and $^1A_1''$ states predicted for $J_\pi = 0$, is not observed. The $^1E'$ state is expected to have strong MCD with $g_z \simeq 4k$. The absorption near 15 300 cm^{-1} is a likely candidate for the $^1E'$ level. The observed g factor gives $4k \sim 0.6$–1.0, which is consistent with the Zeeman analysis of the sharp lines near 7800 cm^{-1}. In order to raise $^1E'$ ~2000 cm^{-1} above the $^1A_1'$ state our model requires a large value for J_π. Figure 9 shows that for $J_\sigma = 15000$ cm^{-1} and $J_\pi = 3750$ cm^{-1}, $E(^1E',{}^1A_1') \simeq 1400$ cm^{-1}, $E(^3E',{}^3E'') \simeq 1000$ cm^{-1} and $E_{10} \simeq 1000$ cm^{-1}. However we have no evidence for a $^3E'$ state lying above 7800 cm^{-1}. The separation between $^1E'$ and $^1A_1$ states is increased further for $J_\pi = J_\sigma$, but now E_{10} becomes much larger than the experimental value of 840 cm^{-1} (Figure 10).

It is evident that within the kinetic approximation the pair model cannot account for the splittings of both the ground and the doubly excited states. Perhaps the neglect of e_g orbitals is not justified for the higher energy levels. The available spectroscopic data suggests that $J_\sigma \simeq 15000$ cm^{-1} and J_π is very small.

Table III compares the observed and calculated energies for $J_\sigma = 15000$ cm^{-1} and small J_π. If the ground multiplet is ignored, the lowest excited state is always $^3E''$ (see Figures 8–10). The splitting between $^3E''$ and the next level $^3E'$ depends both on J_π and $(J_\pi J_\sigma)^{1/2}$. The multiplet separations are reasonably accounted for. However, as mentioned above, the splittings of the doubly excited states cannot be reproduced.

Table IV. Structural Parameters for $A_3M_2Cl_9$ Compounds

	M–M, Å	M–X–M, deg	d', Å	d'',[a] Å
$Cs_3Cr_2Cl_9$[b]	3.12	76.5	1.56	1.27
$Cs_3Mo_2Cl_9$	2.66	64.5	1.33	1.36
$Cs_3W_2Cl_9$	2.50	61.4	1.25	1.33
$K_3Mo_2Cl_9$	2.52	60.6	1.26	1.37
$K_3W_2Cl_9$	2.41	58.1	1.21	1.35

[a] The distances of the metal ion from the planes of the bridging and terminal ligands are denoted by d' and d'', respectively. [b] Data obtained from the single-crystal X-ray structures for $Cs_3Cr_2Cl_9$,[1] $Cs_3Mo_2Cl_9$,[3] and $K_3W_2Cl_9$.[2] Data for $Cs_3W_2Cl_9$ and $K_3Mo_2Cl_9$ were obtained from a Rietveld refinement of X-ray powder data.[31]

Ground Splitting. For $J_\sigma = 15000$ cm^{-1} and $J_\pi = 0$ the calculated singlet–triplet separation is $E_{10} \simeq 530$ cm^{-1}, which accounts for 70% of the observed value. The exchange-coupled $^4A_2{}^4A_2$ model predicts $E_{10} \simeq J_\sigma/9 \simeq 1600$ cm^{-1}. The difference arises from the mixing between $^4A_2{}^4A_2$ and $^4A_2{}^2T_{1z}$ and $^2T_{1z}{}^2T_{1z}$ pair states, which tends to pair off the t_{2z} electrons. For $J_\sigma > 2000$ cm^{-1} and $J_\pi = 0$ the ground multiplet follows the Landé interval rule for a $S_a = S_b = 1$ exchange-coupled pair. The splitting E_{10} reaches a maximum value of ~530 cm^{-1} for $J_\sigma = 15000$ cm^{-1} and then drops slowly to zero as $J_\sigma \rightarrow \infty$. Thus the t_{2z} electrons are fully paired only in the limit $J_\sigma \rightarrow \infty$. For $J_\sigma \simeq 15000$ cm^{-1}, the t_{2z} electrons are only partially paired and kinetic exchange between t_{2z} electrons still gives a large contribution to E_{10}. The influence of J_π on E_{10} is illustrated in Figures 9–10.

One can show that in the $t_{2e}{}^2t_{2e}{}^2$ model, where the t_{2z} electrons are fully paired, the ground splitting is $E_{10} \simeq -2J(x,x)/2 \simeq J_\pi/18$ and the splitting of the lowest excited states is $E(^3E',{}^3E'') \simeq J_\pi/9$. This model requires an unreasonably high value for J_π, ~(18 × 840) cm^{-1}, and a splitting of ~1600 cm^{-1}, which is not observed. The $t_2^3t_2^3$ calculations give the important result that it is possible to have a moderately large value for E_{10} and still have a small splitting of the $^3E'$ and $^3E''$ states.

M–M Bonding in $A_3M_2X_3$ Complexes. It has been customary[4] to view M–M bonding in $Mo_2Cl_9^{3-}$ as an intermediate between that of $Cr_2Cl_9^{3-}$ and that of $W_2Cl_9^{3-}$. Indeed some workers[7] have proposed no bonds in $Cr_2Cl_9^{3-}$, one bond in $Mo_2Cl_9^{3-}$, and three bonds in $W_2Cl_9^{3-}$. This analysis is based on the M–M distances of 2.65 and 2.41 Å observed for $Cs_3Mo_2Cl_9$ and $K_3W_2Cl_9$, respectively. However the six halogen ligands impose a strong cubic field on the metal d orbitals and force the unpaired spins into t_2 orbitals that are not optimized for M–M π-bonding. The π M–M bonds in $Mo_2Cl_9^{3-}$ and $W_2Cl_9^{3-}$ should be very weak. Further evidence for the minor difference in M–M bonding between second- and third-row elements is found in $Nb_2Br_6(SC_4H_8)_3$ and $Ta_2Br_6(SC_4H_8)_3$, which have the confacial bioctahedron structure and M–M distances of 2.73 and 2.71 Å, respectively.[30]

Previous analysis did not consider the influence of the cations on the structure of $M_2X_9^{3-}$. Some time ago Grey and Smith[5] have suggested that a decrease in cation size reduces the M–M separation. Recent work[31] has confirmed this relationship and has emphasized the three-dimensional character of the $A_3M_2X_9$ structure where the cations and X^- form closed packed layers of AX_3 composition. Some of the new structural data is given in Table IV. If the cation is fixed, then the differences in the structure parameters for $Mo_2Cl_9^{3-}$ and $W_2Cl_9^{3-}$ are relatively small. It seems more useful to describe the M–M bonding in the Mo and W compounds as consisting of one strong σ bond and two weak π interactions. We suggest that $Cs_3W_2Cl_9$ may have a low-lying $S = 1$ ground level. The observed diamagnetism[6] at 298 K gives only a lower limit to the singlet–triplet separation, $E_{10} > 1300$ cm^{-1}.

(29) Güdel, H.; Dubicki, L. *Chem. Phys.* **1974**, *6*, 272.
(30) Templeton, J. L.; Dorman, W. C.; Clardy, J. C.; McCarley, R. E. *Inorg. Chem.* **1978**, *17*, 1263.
(31) Stranger, R.; Grey, I. E.; Madsen, I. C.; Smith, P. W. J. *Solid State Chem.*, in press.

Table V. Exchange Parameters for $^4A_2{}^2E$, $^4A_2{}^2T_1$, and $^4A_2{}^2T_2$ States

ΓM	$\Gamma'M'$	$-2J(\Gamma M,\Gamma'M')$	$-2K(\Gamma M,\Gamma'M')$
$^4A_2$	$^4A_2$	A	
$^2E_{u\pm}$	$^2E_{u\pm}$	A	$3B$
$^2E_{u\pm}$	$^2T_{1a\pm}$	$\mp i2^{1/2}C$	$\mp i3(2^{1/2}D)$
$^2T_{1a0}$	$^2T_{1a0}$	$A - 2C$	$3(K + L)$
$^2T_{1a\pm}$	$^2T_{1a\pm}$	$A + C$	$3(M + N)$
$^2T_{2x0}$	$^2T_{2x0}$	$A + 2C$	$-3(K - L)$
$^2T_{2x\pm}$	$^2T_{2x\pm}$	$A - C$	$-3(M - N)$

Conclusions

The electronic spectrum of $Cs_3Mo_2Cl_9$ is characterized by a number of low-energy multiplets with relatively sharp absorption lines. This is good evidence for intraconfigurational transitions of the type $t_2 \nleftrightarrow t_2$, and the adoption of the exchange-coupled chromophore provides a satisfying qualitative description.

Thus Figure 8 demonstrates that large J_σ stabilizes only a restricted set of levels. The corresponding transition energies are relatively insensitive to J_σ, and the absorption lines are expected to be sharp.

Our conclusion that J_π is small is based on the assumption that the lines at 7808 (σ) and 7813 (π) cm^{-1} are true origins and therefore must belong to the $^3E''$ and $^3E'$ states (Table II). Since no other multiplets are observed in the range 7800–4000 cm^{-1} and 7800–11 600 cm^{-1}, the assignment of the $^3E''$ state is firmly established. Some doubt remains for the $^3E'$ assignment as we have not been able to dismiss the possibility that the π line is a vibronic.

The observed distribution of multiplets roughly follows the $t_{2e}{}^2t_{2e}{}^2$ model. This extreme case requires unreasonably large values for J_π and large $E(^3E',^3E'')$. The full $t_2{}^3t_2{}^3$ calculation remedies this defect and shows that the electrons which are approximately paired off may still contribute significantly to the splitting of the ground multiplet. However these calculations cannot account for the splittings of both the ground and the doubly excited multiplets with a single set of J_σ and J_π parameters.

Acknowledgment. We thank Dr. Ian Grey of Mineral Chemistry, CSIRO, Melbourne, Australia, and Professor Hans Güdel of the University of Bern for providing preprints of their papers, ref 31 and 35.

Appendix 1. Energy Matrix for the $t_2{}^3t_2{}^3$ Configuration

Real trigonal t_2 obtials were chosen in order to take advantage of the tabulated vector coupling and fractional parentage coefficients.[28] A computer program generated the single ion functions, $|t_2{}^3\Gamma\gamma Sm_s\rangle$, and coupled them to form the pair states $|\Gamma_aS_a\Gamma_bS_b\Gamma\gamma SM_s\rangle$. The reduced matrix elements of $S(\alpha\alpha')$ and $n(\alpha\alpha')$ were evaluated and stored as suitably indexed variables. The Wigner–Eckart theorem[28] was then used to calculate the matrix elements of $S_a(\alpha\alpha')\cdot S_b(\beta\beta')$, $n_a(\alpha\alpha')n_b(\beta\beta')$ and $n_a(\alpha\alpha')$. The number of parameters was reduced by invoking the "kinetic approximation". The energy matrix contained the exchange parameters J_σ, J_π, and $(J_\sigma J_\pi)^{1/2}$ and also the electron repulsion energies $E(^2E) = 9B + 3C - 90B^2/10Dq$, $E(^2T_1) = 9B + 3C - 24B^2/10Dq$, and $E(^2T_2) = 15B + 5C - 176B^2/10Dq$. The order of matrix was 164 and was reduced by forming linear contributions of $|\Gamma\gamma SM_s\rangle$, which formed bases for the irreducible representation of the D_{3h} point group. The reflection operators, σ_{ho} (operating on orbital variables) and σ_{hs} (spin) were used to classify the pair states

$$\sigma_{h0}|SM_s\rangle = (-)^{S_a+S_b-S+1}|SM_s\rangle$$

$$\sigma_{h0}\sigma_{hs}|SM_s\rangle = (-)^{S+M_s}|SM_s\rangle$$

$$\sigma_{h0}|\pm\Gamma\gamma SM_s\rangle = (\pm)(-)^{S_a+S_b'-S+1}|\pm\Gamma\gamma SM_s\rangle$$

$$\sigma_{h0}\sigma_{hs}|\pm\Gamma\gamma SM_s\rangle = (\pm)(-)^{S_a+S_b'+S+M_s+1}|\pm\Gamma\gamma SM_s\rangle$$

where $|SM_s\rangle = |A_2S_aA_2S_bSM_s\rangle$, $S_a = S_b = {}^3/_2$, and $|\pm\Gamma\gamma SM_s\rangle = (1/2^{1/2})\{|\Gamma_aS_a\Gamma_b'S_b'\Gamma\gamma SM_s\rangle \pm |\Gamma_a'S_a'\Gamma_bS_b\Gamma\gamma SM_s\rangle\}$, where $S_a = S_b$ and $S_a' = S_b'$ take the values ${}^1/_2$ or ${}^3/_2$.

The energy matrix was blocked out into $^1A_1'(9)$, $^1A_2'(4)$, $^1E'(12)$, $^1A_1''(7)$, $^1A_2''(3)$, $^1E''(9)$, $^3A_1'(4)$, $^3A_2'(8)$, $^3E'(12)$, $^3A_1''(5)$, $^3A_2''(10)$, $^3E''(15)$, $^5A_1'(2)$, $^5A_1'(1)$, $^5E'(3)$, $^5A_1''(1)$, $^5A_2''(1)$, $^5E''(3)$, and $^7A_1'(1)$ matrices. The pair energies were calculated as a function of J_σ and J_π (Figures 8–10). During the course of this work we became aware of a more sophisticated use of tensor methods in diagonalizing $\mathbf{H}_{ex}$. Extending the methods of Błaszak[32] and Eremin et al.[33] to our problem, we were able to reproduce, more efficiently, the results in Figures 8–10. Details on this calculation are available from R.S.

Appendix 2. Trigonal d^3d^3 Pairs with Weak M–M Bonding

In contrast to $Mo_2Cl_9{}^{3-}$, the dimers with metal ions of the 3d series have often weak M–M bonding as well as larger Racah parameters. In these cases the mixing between singly and doubly excited states is very small, and the exchange splittings for the $^4A_2{}^2E$, $^4A_2{}^2T_1$ and $^4A_2{}^2T_2$ states, all based on the $t_2{}^3$ configuration, can be obtained by diagonalizing $\mathbf{H}_{ex}$ within the singly excited manifold. The exchange splittings should be determined by the spin-dependent terms in $\mathbf{H}_{ex}$. The diagonal matrix elements of the spin-independent terms are the same for all states while the off-diagonal elements connecting $^4A_2{}^2T_{2\pm}$ and $^4A_2{}^2E_\pm$ can be ignored since they are much smaller than the energy separation $E(^2T_2,^2E) \simeq 6B + 2C$. The required matrix elements have been tabulated[23] but Table III in ref 23 contains errors. In this appendix, the errors are corrected and the exchange parameters, originally given in a real cubic basis, are now expressed in the more convenient complex trigonal basis.

The relationship between complex trigonal, real cubic and real trigonal bases is

$$t_{2x\pm} = \mp(\omega^{\pm}\xi + \omega^{\mp}\eta + \zeta)/3^{1/2} = \mp(t_{2x} \pm it_{2y})/2^{1/2}$$

$$t_{20} = (\xi + \eta + \zeta)/3^{1/2} = t_{2z}$$

$$e_{u\pm} = \mp(u \pm iv)/2^{1/2} = \mp(e_x \pm ie_y)/2^{1/2} \qquad \text{(A2.1)}$$

The singly excited states are denoted by

$$|\pm\Gamma MSM_s\rangle = \{|A_2S_a\Gamma_bM_bS_b'SM_s\rangle \pm |\Gamma_aM_aS_a'A_2S_bSM_s\rangle\}/2^{1/2} \qquad \text{(A2.2)}$$

where $S_a = S_b = {}^3/_2$, $S_a' = S_b' = {}^1/_2$ and ΓM denotes ^2E, $^2T_1$, and $^2T_2$ states. The matrix elements of $\mathbf{H}_{ex}$ are

$$\langle\pm\Gamma MSM_s|\mathbf{H}_{ex}|\pm\Gamma'M'SM_s\rangle = -2J(\Gamma M,\Gamma'M') \times (S(S+1) - {}^9/_2)/2 \pm -2K(\Gamma M,\Gamma'M')\,S(S+1)/12$$

$$\langle A_2S_aA_2S_bSM_s|\mathbf{H}_{ex}|A_2S_aA_2S_bSM_s\rangle = -2J(A_2,A_2)(S(S+1) - {}^{15}/_2)/2 \qquad \text{(A2.3)}$$

where the factor of -2 arises because we now use the notation given in (1). Table V lists the nonvanishing parameters for D_{3h} pair symmetry.

The parameters, A, B, ..., N, have been expressed[23] in terms of real cubic $J_{ik,jl}$, and now must be multiplied by -2, e.g. $A = -2(J_{11} + 2J_{12})/3$. The latter can be transformed into the complex trigonal basis by the following nonorthogonal matrix

$$\begin{bmatrix} J_{11} \\ J_{12} \\ J_{11,12} \\ J_{11,23} \\ J_{12,12} \\ J_{12,21} \\ J_{12,23} \\ J_{12,32} \end{bmatrix} =$$

$$\frac{1}{9}\begin{bmatrix} 2 & 1 & 2 & 4 & 2 & \pm 8 & 4 & -4 \\ 2 & 1 & 2 & 4 & -1 & \mp 4 & -2 & 2 \\ -1 & 1 & -1 & 1 & -1 & \mp 1 & 1 & -1 \\ -1 & 1 & -1 & 1 & 2 & \pm 2 & -2 & 2 \\ -1 & 1 & 2 & -2 & 2 & \mp 4 & -2 & -4 \\ 2 & 1 & -1 & -2 & 2 & \mp 4 & 4 & 2 \\ -1 & 1 & 2 & -2 & -1 & \pm 2 & 1 & 2 \\ 2 & 1 & -1 & -2 & -1 & \pm 2 & -2 & -1 \end{bmatrix}\begin{bmatrix} J(x\pm,x\pm) \\ J(xo,xo) \\ J(x\pm,x\mp) \\ J(x\pm,xo) \\ J(x\pm\ x\mp,x\mp x\pm) \\ J(x\pm\ x\mp,x\pm xo) \\ J(x\pm xo,xox\pm) \\ J(x\pm xo,x\mp xo) \end{bmatrix}$$

(32) Błaszak, M. *Acta Phys. Pol. A* **1980**, *A51*, 491, 503.
(33) Eremin, M. V.; Kalinenkov, V. N.; Rakitin, Y. U. *Phys. Status Solidi B* **1978**, *90*, 123.

For example, we obtain

$$A = -2(2J(x\pm,x\pm) + 2J(x\pm,x\mp) + 4J(x\pm,x0) + J(x0,x0))/9 \quad \text{(A2.4)}$$

If the kinetic approximation (eq 8) is valid, then

$$A \simeq (2J'_\pi + J_\sigma)/9$$

$$B \simeq (J'_\pi + 2(J_\sigma J'_\pi)^{1/2})/9$$

$$C \simeq (-J'_\pi + J_\sigma)/9$$

$$D \simeq (J'_\pi - (J_\sigma J'_\pi)^{1/2})/9$$

$$3(K + L) \simeq (J'_\pi + 2J_\sigma)/3$$

$$3(M + N) \simeq (2J'_\pi + (J_\sigma J'_\pi)^{1/2})/3$$

$$-3(K - L) \simeq J'_\pi$$

$$-3(M - N) \simeq (J_\sigma J'_\pi)^{1/2} \quad \text{(A2.5)}$$

where $J'_\pi = J_\pi/9 = 4h(x\pm,x\pm)^2/U$, and we have assumed that the transfer integrals $h(x\pm,x\pm) = h(x,x)$ and $h(x0,x0) = h(z,z)$ have the same sign.

Using eq A2.5 and A2.3, one can show that large J_σ causes extensive mixing between $^4A_2{}^2E_{u\pm}$ and $^4A_2{}^2T_{1a\pm}$ states. This is precisely what is observed in tris(μ-hydroxo)bis(1,4,7-trimethyl-1,4,7-triazacyclononane)chromium(III) ion.[34,35]

In order to derive the eigenvalues it is necessary to include single-ion Coulombic and trigonal perturbations that remove the quasi-degeneracy of the $^2T_1$ and ^2E states and also produce zero-field splittings. The simplest procedure is to introduce an empirically derived energy separation $E(^2T_1,{}^2E)$ and determine the zero field splittings with the effective Hamiltonians[36]

$$\mathbf{H}(^2E) = -D(^2E)S_zT_z$$

$$\mathbf{H}(^2T_1) = -F(^2T_1)(3T_z^2 - T(T+1)) + \lambda_0 S_zT_z + \lambda(S_xT_x + S_yT_y) \quad \text{(A2.6)}$$

where $D(^2E) = E(\mp^1/_2u\pm) - E(\pm^1/_2u\pm)$, and F, λ_0, and λ are the effective trigonal field and spin–orbit parameters for the $^2T_1$ multiplet. $D(^2E)$ is mainly determined by the trigonal field parameter[37] v while $F(^2T_1)$ is more sensitive[38] to v'. In fact we find[38] that $F(^2T_1) \simeq -v'/10$. The parameters λ and λ_0 are complicated functions of v and v'. For large $|v'|$ the zero-field splitting of the $^2T_1$ state is mainly determined by $F(^2T_1)$, and as a first approximation λ and λ_0 may be neglected.

We now consider in more detail the single-ion perturbations in the tris(hydroxo) complex.[34] The structural data[39] for the iodide salt gives the bond lengths, r(Cr–O) = 1.97 Å, r(Cr–N) = 2.09 Å, and r(Cr–Cr) = 2.64 Å. The polar angle, with respect to the C_3 axis, for the bridging oxygen atoms is $\theta_b = 48.0°$, and for the terminal nitrogen atoms, $\theta_t = 50.5°$. Hence the Cr(III) ion has two strong "elongated" trigonal fields as well as an axial field generated by the second Cr(III) ion.

The observed zero-field splitting in the ground multiplet is nearly all due to single-ion anisotropy[34] and $D(^4A_2) = (\pm^1/_2) - (\pm^3/_2) \simeq -1.8$ cm^{-1}. This value is similar to that for Cr^{3+}:$ZnAl_2O_4$ (spinel),[37] where $D(^4A_2) = -1.86$ cm^{-1}. Macfarlane[37] has shown that for Cr(III) doped in oxide lattices, $D(^4A_2)$ varies linearly with v' and v' $\simeq -1700$ cm^{-1} for $ZnAl_2O_4$. For the hydroxo dimer we expect[38] that $F(^2T_1) \simeq +170$ cm^{-1}, so that $E(^2T_{10}) - E(^2T_{1\pm}) \simeq +510$ cm^{-1}, which agrees with the empirical value[35] of +450 cm^{-1}.

The bridging angles and bridging bond lengths in the hydroxo dimer are almost identical with those in the 1*nn* pair in ruby.[40] It is therefore not surprising to find that the ground exchange parameters are very similar for the two pairs.[34] However, the single-ion perturbations should be significantly different. For example in ruby the terminal oxygen atoms[40] have $\theta_t = 63.1°$ and r(Al–O) = 1.86 Å, and contribute a large "compressed" trigonal field. Calculations,[38] based on the linear ligator AOM[41] model and including the axial field of the second Cr(III) ion, suggest that v' $\simeq -1800$ cm^{-1} and v $\simeq -1000$ cm^{-1} for the hydroxy dimer. For ruby, Macfarlane[37] gives $D(^4A_2) = +0.38$ cm^{-1}, v' = +680 cm^{-1} and v = +800 cm^{-1}.

Registry No. $Cs_3Mo_2Cl_9$, 29013-02-3.

(34) Riesen, H.; Güdel, H. U.; Chaudhuri, P.; Wieghardt, K. *Chem. Phys. Lett.* **1984**, *110*, 552.
(35) Riesen, H.; Güdel, H. U.; Chaudhuri, P.; Wieghardt, K. *Mol. Phys.*, in press.
(36) Sugano, S.; Tanabe, Y. *J. Phys. Soc. Jpn.* **1958**, *13*, 880.
(37) Macfarlane, R. M. *Phys. Rev. B: Solid State* **1970**, *1*, 989.
(38) Dubicki, L.; Hauser, A., submitted for publication.
(39) Wieghardt, K.; Chaudhuri, P.; Nuber, B.; Weiss, J. *Inorg. Chem.* **1982**, *21*, 3086.
(40) Macfarlane, R. M. *Phys. Rev. B: Solid State* **1971**, *3*, 2129.
(41) McClure, D. S. *J. Chem. Phys.* **1963**, *38*, 2289.
(42) Schaffer, C. E. *Proc. R Soc. London, A* **1968**, *297*, 96.

Contribution from the Department of Chemistry, University Center at Binghamton, State University of New York, Binghamton, New York 13901

Isolation and Characterization of Novel Photoproduced $M(CO)_5(en)$ Complexes (M = Cr, Mo, W; en = Ethylenediamine)

David E. Marx and Alistair J. Lees*

Received December 5, 1986

Novel monodentate $M(CO)_5(en)$ complexes, where M = Cr, Mo, W and en = ethylenediamine, are formed on UV photolysis of $M(CO)_6$ solutions containing en. These compounds have been isolated and characterized by infrared and electronic absorption spectroscopy and by elemental analyses. The $M(CO)_5(en)$ complexes undergo chelation via a first-order kinetic process to form $M(CO)_4(en)$ and CO products. Determined reaction rates of $M(CO)_5(en)$ are as follows: 3.0×10^{-4} s^{-1} (for M = Cr at 323 K), 3.5×10^{-4} s^{-1} (for M = Mo at 298 K), and 4.2×10^{-5} s^{-1} (for M = W at 323 K). The order Mo > Cr > W is consistent with that of the reactivity and calculated M–C force constants of $M(CO)_6$ complexes in solution. Light irradiation of $M(CO)_5(en)$ solutions that contain an excess concentration of PPh_3 result in substitution of the unique ligand and formation of $M(CO)_5(PPh_3)$ products.

Introduction

Ethylenediamine (en) is an important ligand and is known to undergo bidentate coordination with a wide range of transition-metal centers. Indeed, metal complexes containing the en ligand have been studied extensively and over 5700 papers on this subject have appeared in the literature since 1968.[1] Only a few of these studies have characterized reaction intermediates in which en is

(1) Results obtained from a computer-generated search of *Chemical Abstracts*, using the CAS Online service.

0020-1669/87/1326-2254$01.50/0